JOURNAL OF SOLID STATE CHEMISTRY **141,** 212–220 (1998)
ARTICLE NO. SC987958

Synthesis, Crystal Structure, and Magnetic Properties of $La_4Co_3O_{10+\delta}$ ($0.00 \leq \delta \leq 0.30$)

Ole Henrik Hansteen and Helmer Fjellvåg[1]

Department of Chemistry, University of Oslo, N-0315 Oslo, Norway

Received January 28, 1998; in revised form June 25, 1998; accepted July 6, 1998

The effects of nonstoichiometry on the crystal structure, thermal expansion, structural phase transitions, and magnetic properties of $La_4Co_3O_{10+\delta}$, $0.00 \leq \delta \leq 0.30$, have been investigated between 2 and 1000 K. Rietveld analysis of high resolution powder X-ray diffraction data reveals the crystal structure of $La_4Co_3O_{10+\delta}$ (Ruddlesden–Popper type phase; $La_{n+1}Co_nO_{3n+1}$ with $n=3$) to be slightly monoclinically distorted, space group $C2/m$. The monoclinic distortion increases and the unit cell volume decreases slightly on increasing nonstoichiometry, δ. A structural phase transition, monoclinic to tetragonal, possibly via an intermediate orthorhombic state, occurs at 840 K. Magnetic susceptibility data indicate long-range antiferromagnetic ordering below $T_N \approx 13$ K. Above 20 K there are three temperature regimes with nearly Curie–Weiss paramagnetic behaviour for the magnetic susceptibility: 20–80 K, 100–450 K, 650–985 K. This indicates a temperature-induced change from a lower, possibly via an intermediate, to a higher spin configuration for Co^{III} comparable to that described for $LaCoO_3$. Field-dependent magnetic susceptibility is observed for $\delta > 0.00$ for $T < 100$ K.

INTRODUCTION

In the La-Co-O system phases belonging to the homologous series $La_{n+1}Co_nO_{3n+1}$ (alternatively $LaO(LaCoO_3)_n$) are known for the compositions La_2CoO_4 ($n = 1$; K_2NiF_4-type), $La_4Co_3O_{10}$ ($n = 3$) and $LaCoO_3$ ($n = \infty$; perovskite-type). The crystal structures of these phases are of the Ruddlesden–Popper (RP) type (1). The Ruddlesden–Popper type structure can ideally be described by the stacking of n two-dimensional perovskite-type sheets of corner-sharing CoO_6-octahedra along the crystallographic c-direction into layers $(LaCoO_3)_n$, which are separated by a single NaCl-type LaO layer. The NaCl-type layers are related to a translation of successive perovskite layers by 1/2 in the [1 1 0] direction of the ideal tetragonal unit cell. Similar RP-type phases $A_{n+1}M_nO_{3n+1}$ are known for a variety of oxide systems, where A usually is a rare-earth, alkaline-earth or alkali element and M is a 3*d* or 4*d* transition element. In recent years there has been a large interest in the related La-*M*-O systems, M = Ni or Cu (2–6), the main reason being high-temperature superconductivity for the Cu-phases and the close structural and mixed-valence similarities of the RP-phases in the Ni system.

The phase relations in the La-Co-O system as a function of temperature (T) and partial oxygen pressure ($p(O_2)$) have been studied by several groups (7–9), and extensive studies on the structure, nonstoichiometry, thermal, thermodynamic, electric, and magnetic properties of the two end-phases of the RP-series, La_2CoO_4 and $LaCoO_3$, have been reported (10–20). So far the intermediate phase $La_4Co_3O_{10\pm\delta}$ has attracted little attention. The phase was first reported by Seppänen and Tikkanen (21) who proposed the structure to be of an *F*-centered orthorhombically modified RP-phase. Stoichiometric $La_4Co_3O_{10}$ is obtained in pure N_2 atmosphere ($p(O_2) \approx 10$ Pa). Le Coustumer *et al.* (22) showed that nonstoichiometric $La_4Co_3O_{10+\delta}$, $0.00 \leq \delta \leq 0.28$, can be obtained via monitoring of the $p(O_2)$. Oxygen nonstoichiometry is present in all phases of this RP-system, owing to the possibility of mixed valence for cobalt ($Co^{II}(d^7)$ and $Co^{III}(d^6)$), and it has been shown that the oxygen nonstoichiometry is strongly dependent on temperature and $p(O_2)$. For $La_4Co_3O_{10+\delta}$, larger δ means that the fraction of Co^{III} with the d^6 configuration increases. A structural phase transition, orthorhombic to tetragonal, is reported at 848 K (22) and a magnetic/electronic phase transition occurs in the temperature range 400–600 K (23). The transition is believed to be a semiconductor to metal transition. The magnetic susceptibility follows the Curie–Weiss law both in the temperature range below and above the transition. In this respect $La_4Co_3O_{10}$ shows interesting similarities to the intriguing $LaCoO_3$ phase (11, 14).

The present study focuses on the effects of nonstoichiometry on the crystal structure, thermal expansion, structural phase transitions, and magnetic properties of $La_4Co_3O_{10+\delta}$ between 2 and 1000 K. In order to clarify the slight structural deformations of the crystal structure, high

[1]Corresponding author.

0022-4596/98 $25.00

resolution powder X-ray diffraction data from ESRF have been collected and analysed.

EXPERIMENTAL

Synthesis from citrate solutions. The starting materials for the synthesis were La_2O_3 (99.99%, Molycorp), $Co(CH_3COO)_2 \cdot 4H_2O$ (> 99%, Fluka), and citric acid monohydrate, $C_3H_4(OH)(COOH)_3 \cdot H_2O$ (> 99.8%, Riedel-de Haën). La_2O_3 was calcined in air at 1273 K to remove any water and carbon dioxide. The Co content of $Co(CH_3COO)_2 \cdot 4H_2O$ was determined gravimetrically. La_2O_3 was dissolved in concentrated HNO_3 before adding the citric acid (weight ratio 1:30). A clear solution was obtained which was left boiling until all nitrates were removed as nitrous gases. $Co(CH_3COO)_2 \cdot 4H_2O$ was added along with distilled water. The citrate solution was dehydrated at 450 K and carbonaceous species in the resulting X-ray amorphous xerogel were removed by incineration at 720 K. The fine, dark grey powder was cold-pressed into pellets, placed in an alumina crucible, and calcined under flowing nitrogen ($p(O_2) = 10$ Pa) at 1300 K for 110 h with two intermediate grindings followed by repelletization. Dependent on the cooling and storage conditions three samples of $La_4Co_3O_{10+\delta}$ with different oxygen content (δ) were prepared: (i) $\delta = 0.00$, cooled in the furnace (2 K min^{-1}) from 1300 K under flowing nitrogen; (ii) $\delta = 0.07$, as (i), but with subsequent six months storage in a desiccator at ambient temperature, allowing a slow oxidation at very mild conditions. No broadening of the PXD reflections were observed, hence the sample is most probably homogenously oxidized. Such spontaneous slow oxidation at room temperature has earlier been reported for La_2CoO_4 (24); (iii) $\delta = 0.30$, taken out of the furnace ($T = 1300$ K) directly into air. The oxygen contents were determined gravimetrically by oxidizing the samples completely in pure oxygen atmosphere at 1300 K to yield stoichiometric $LaCoO_3$ plus La_2O_3 (nominal composition of final two-phase mixture is $La_4Co_3O_{10.50}$). Phase purity was assured from powder X-ray diffraction.

Powder X-ray diffraction (PXD). Room temperature PXD data were collected with a Guinier Hägg camera using Si as internal standard ($a = 543.1065$ pm). Both Cr$K\alpha_1$ (detection limit for impurities ca 0.3 wt% (25)) and Cu$K\alpha_1$ radiation were used. Additional data were collected with a Siemens D500 diffractometer, Cu$K\alpha_1$ radiation. Unit cell dimensions were determined by least squares calculations using the program UNITCELL (26). Synchrotron PXD data were collected for $La_4Co_3O_{10.00}$ and $La_4Co_3O_{10.30}$ with the powder diffractometer in Debye–Scherrer mode at the Swiss Norwegian Beam Line (BM1) at ESRF (Grenoble, France). Monochromatic X-rays were obtained from a channel-cut Si(111) crystal. X-rays of wavelength 109.803 and 89.987 pm were used for the two samples, respectively. The samples were contained in rotating silica glass capillaries (diameter 0.2 and 0.5 mm, respectively). Intensity data were collected at 298 K between $2\theta = 10$ and 60° in steps of $\Delta(2\theta) = 0.007°$. The GSAS program package (27) was used for the Rietveld-type profile refinements. Table 1 summarizes characteristic features of the data sets and the variable parameters entering into the least-squares refinements. The atomic parameters for orthorhombic $La_4Ni_3O_{10}$ (space group *Fmmm*) (5) were used as a starting model. The background was modelled by a cosine Fourier series. The peak shape was modelled by a pseudo-Voigt function using three Gaussian half-width parameters (U, V, W) and three Lorentzian coefficients (two Scherrer broadening coefficients and one strain broadening coefficient).

High temperature PXD data were collected upon continuous heating by a Guinier Simon camera (Enraf Nonius), Cu$K\alpha_1$ radiation. The samples were kept in rotating silica-glass capillaries, either sealed and evacuated or open to the air. Photographic film was used as the detector and the temperature change was synchronized with the movement of the film cassette. The temperature was calibrated by means of measurement of the thermal expansion of silver (28).

Thermal analysis. Thermogravimetric (TGA) and differential thermal (DTA) analysis in nitrogen, air, and oxygen atmospheres were performed with a Perkin Elmer, TGA7 and DTA7, and by differential scanning calorimetry (DSC) using a Mettler TA 3000 system. Data reduction was performed with standard programs for the systems.

Magnetic measurements. Magnetic susceptibility data were measured by a Quantum Design SQUID-magnetometer (MPMS) in the temperature range 2–300 K (magnetic field, $H \leq 10.0$ kOe). All samples were zero field cooled and

TABLE 1
Characteristic Features of the Synchrotron X-Ray Diffraction Data Sets and the Parameters Entering the Profile Refinements

	$La_4Co_3O_{10.00}$	$La_4Co_3O_{10.30}$
Data points	6371[a]	7136
Reflections (hkl)	462	694
Scale factor	1 + 1[a]	1
Zero point	1 + 1[a]	1
Profile parameters	5 + 5[a]	6
Unit cell dimensions	4	4
Positional parameters	12	12
Isotropic displacement factors	3	3
Background coefficients	6 + 5[a]	6
Refinable parameters	44	33

[a] The data set consists of two parts which are refined simultaneously and therefore doubling of certain parameters are required.

the temperature dependence of the magnetic susceptibility was measured on heating. A Faraday balance was used in the temperature range 300–970 K ($H \leq 7.0$ kOe) and the magnetic susceptibility was measured both on heating and cooling. The samples were held in gelatine capsules and spherical silica glass ampoules for the two methods, respectively. The measured magnetic susceptibility was corrected for the diamagnetic contribution from the sample containers and from core electrons.

RESULTS AND DISCUSSION

(i) Crystal Structure

The Guinier Hägg PXD patterns at 298 K for the three samples of $La_4Co_3O_{10+\delta}$ with different oxygen contents were almost identical. All reflections could satisfactorily be indexed using the *F*-centred orthorhombic unit cell suggested by Seppänen and Tikkanen (21). The obtained unit cell dimensions, $a = 541.4\ (2)$ pm, $b = 547.6\ (2)$ pm, $c = 2777\ (1)$ pm, agreed well with the reported ones (21). No significant variations exceeding the standard deviations were observed in the unit cell dimensions as a function of δ. However, a very small, but significant decrease in the *d*-spacing of (2 2 0) as a function of increasing δ was observed. This clearly indicates a small decrease in unit cell dimensions with increasing oxygen content. (The *d*-spacing of (2 2 0) of $La_4Co_3O_{10+\delta}$ can be precisely determined because of its close proximity to the (2 2 0) for the Si standard.)

A systematic peak broadening is observed for certain reflections in the Guinier Hägg PXD patterns at 298 K. The effect is apparently rather independent of the oxygen content (δ). Inspection of the synchrotron PXD intensity profiles and subsequent Rietveld profile refinements showed a systematic splitting of the orthorhombic reflections of the types (*hkl*) and (*h*0*l*). This suggests that the real symmetry is lower than earlier anticipated for an *F*-centred orthorhombic RP-type unit cell (7, 21). Examples of the peak splitting are given in Fig. 1. The orthorhombic (1 1 7) reflection is clearly resolved into two separate peaks, (1 1 $\bar{7}$) and (1 1 7). The splitting implies a minor monoclinic distortion ($\beta \neq 90^\circ$) of the ideal RP-type atomic arrangement (Table 2). The monoclinic crystal structure of stoichiometric $La_4Co_3O_{10}$ is presently described in space group $C2/m$, a nonisomorphic subgroup of *Fmmm*. No additional reflections indicating lack of *C*-centering were observed. Note, however, that the major scattering contributions come from the heavy La and Co atoms and that small oxygen displacements (e.g. connected with tilting of octahedra) may not be detectable with X-rays. The results of the Rietveld refinements are given in Tables 2 and 3. The *x* and *y* coordinates were fixed to ideal (*Fmmm*) values during the refinements. Introduction of soft constraints on Co-O interatomic

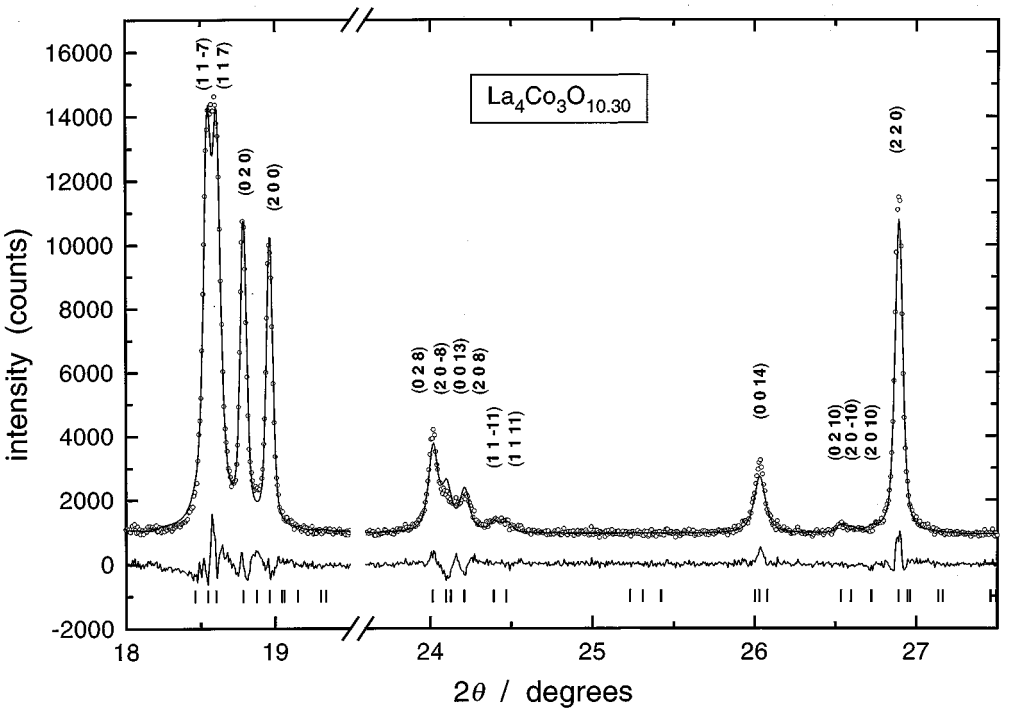

FIG. 1. Selected parts of the synchrotron PXD profile for $La_4Co_3O_{10.30}$ showing monoclinic splitting of certain reflections. Miller indices are given. Experimental points marked by open circles, full line marks calculated profile, lower full line marks difference plot, vertical bars mark positions for reflections. Wavelength $\lambda = 89.987$ pm.

TABLE 2
Crystal Structure Data for $La_4Co_3O_{10+\delta}$

	$La_4Co_3O_{10.00}$	$La_4Co_3O_{10.30}$
Crystal system	Monoclinic	Monoclinic
Space group	*C*2/*m*	*C*2/*m*
a, pm	541.79(1)	541.51(1)
b, pm	547.56(1)	546.46(1)
c, pm	2780.5(1)	2779.2(1)
β, °	90.200(1)	90.264(1)
V, 10^8 pm^3	8.2486(6)	8.2241(4)
Z	4	4
R_p (%)[a]	7.2	5.0
R_{wp} (%)[a]	9.5	6.4
R_{exp} (%)	8.6	3.0
χ^2	1.23	4.44

Note. Calculated standard deviations in parentheses.
[a] $R_p = 100(\sum|I_O - I_C|/\sum I_O)$, $R_{wp} = 100(\sum w(I_O - I_C)^2/\sum wI_O^2)^{-1/2}$.

distances showed that a considerable spread in Co-O distances (and, hence, deformation of the octahedra) initially obtained was not significant. Structure models with only minor deformations of the CoO_6-octahedra were not inferior with respect to *R*-values. The crystal structure for $La_4Co_3O_{10.00}$ is shown in Fig. 2. Translated triple perovskite-type layers, $(LaCoO_3)_3$, characterized by the corner-sharing CoO_6-octahedra are clearly identified between single LaO-layers with NaCl-type arrangement. The CoO_6-octahedra of Co(1) and Co(2) constitute the central sheet of the two triple perovskite-type layers in the unit cell, Fig. 2. La(3) and La(4), which are situated within the perovskite layers, are 12-coordinated with respect to oxygen, just like in $LaCoO_3$, and have La-O distances in the range 269–289 pm. La(1) and La(2), which are situated at the interface between the perovskite layers and LaO-layers, are 9-coordinated due to the relative translation of successive perovskite layers and have La-O distances in the range 245–275 pm.

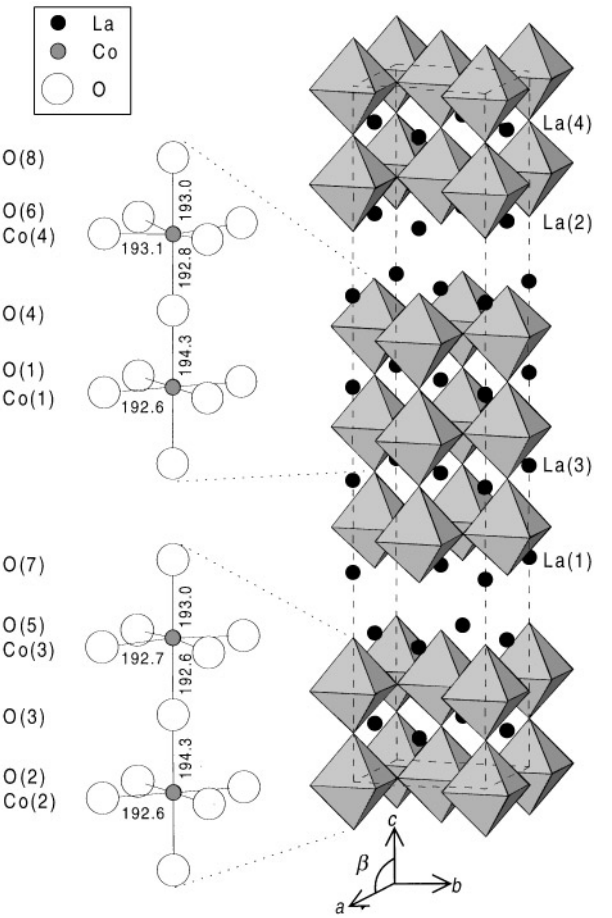

FIG. 2. Crystal structure of stoichiometric $La_4Co_3O_{10.00}$.

TABLE 3
Fractional Atomic Coordinates (*x*, *y*, *z*) for $La_4Co_3O_{10+\delta}$, $\delta = 0.00$ and 0.30

Atom	Wyckoff site[a]	Coordinates	$\delta = 0.00$ *z*	$\delta = 0.30$ *z*
La(1)	4i	(0,0,*z*)	0.301 (1)	0.300 (2)
La(2)	4i	(1/2,0,*z*)	0.801 (1)	0.800 (2)
La(3)	4i	(0,0,*z*)	0.433 (1)	0.432 (1)
La(4)	4i	(1/2,0,*z*)	0.932 (1)	0.931 (1)
Co(1)	2d	(0, 1/2,1/2)		
Co(2)	2a	(0,0,0)		
Co(3)	4i	(0,0,*z*)	0.1391 (1)	0.1388 (2)
Co(4)	4i	(1/2,0,*z*)	0.6392 (1)	0.6388 (2)
O(1)	4f	(1/4,1/4,1/2)		
O(2)	4e	(1/4,1/4,0)		
O(3)	4i	(0,0,*z*)	0.0699 (1)	0.0696 (1)
O(4)	4i	(1/2,0,*z*)	0.5699 (1)	0.5696 (1)
O(5)	8j	(1/4,1/4,*z*)	0.136 (1)	0.137 (5)
O(6)	8j	(3/4,1/4,*z*)	0.6447 (6)	0.639 (5)
O(7)	4i	(0,0,*z*)	0.2086 (2)	0.2083 (3)
O(8)	4i	(1/2,0,*z*)	0.7086 (1)	0.7083 (3)

Note. Space group *C*2/*m*. Refinements for $La_4Co_3O_{10.30}$ were based on the model for stoichiometric $La_4Co_3O_{10.00}$ (see text). Calculated standard deviations in parentheses. Isotropic displacement factors (B_{iso} in 10^4pm^2): B_{iso}(La) = 1.82 (6), B_{iso}(Co) = 0.7 (1), B_{iso}(O) = 3.2 (2) for $\delta = 0.00$; B_{iso}(La) = 1.66 (2), B_{iso}(Co) = 0.26 (7), B_{iso}(O) = 3.9 (2) for $\delta = 0.30$.
[a] The *x* and *y* coordinates for all atoms were fixed and not refined: 2a (0, 0, 0); 2d (0, 1/2, 1/2); 4e (1/4, 1/4, 0); 4f (1/4, 1/4, 1/2); 4i (*x*, 0, *z*); 8j (*x*, *y*, *z*).

The synchrotron PXD data show that a small volume contraction occurs on increasing oxygen content, δ (Table 2), probably owing to an increased amount of the smaller sized Co^{III} (d^6) relative to Co^{II} (d^7). Furthermore, an increase of the monoclinic distortion (β) occurs on increasing oxygen content. A trial model based on the positional ordering of excessive oxygen in the LaO layer as described by Demourgues *et al.* (2) for $La_2NiO_{4.25}$ was tested but failed to describe the oxygen excess in $La_4Co_3O_{10.30}$. The PXD data are strongly dominated by the scattering from the heavy

cations, and neutron and electron-diffraction data are required for a complete structural description. For this reason the structural description of $La_4Co_3O_{10+\delta}$ must still be considered as approximate. The profile refinements for $La_4Co_3O_{10.30}$ were, hence, based on the model for $\delta = 0.00$; cf. Table 3.

For the isostructural phase $La_4Ni_3O_{10}$, Zhang and Greenblatt reported peak broadening (5). Therefore, a single phase sample of $La_4Ni_3O_{10}$ was synthesized from citrate solutions and finally calcined in air at 1340 K. PXD showed a systematic peak broadening for $La_4Ni_3O_{10}$ identical to that described above for $La_4Co_3O_{10+\delta}$. It is, hence, probable that $La_4Ni_3O_{10}$, just like $La_4Co_3O_{10+\delta}$, adopts a slightly monoclinically distorted RP-type crystal structure.

The crystal structures of the three phases of the RP-series in the La-Co-O system are all characterized by lower symmetry than the ideal atomic arrangement of the respective structure types: (i) $LaCoO_3$ is rhombohedrally distorted relative to the cubic perovskite structure (29); (ii) $La_4Co_3O_{10+\delta}$ is monoclinically distorted relative to the tetragonal RP-type structure; and (iii) La_2CoO_4 is orthorhombically distorted relative to the tetragonal K_2NiF_4-type structure (30). For $LaCoO_3$ and La_2CoO_4 the distortion implies tilting of the CoO_6-octahedra relative to the crystallographic axes. Space-group $C2/m$, adopted for $La_4Co_3O_{10+\delta}$, also allows tilting of the CoO_6-octahedra; however, this is only feasible if the x and y coordinates deviate from the presently fixed ideal values.

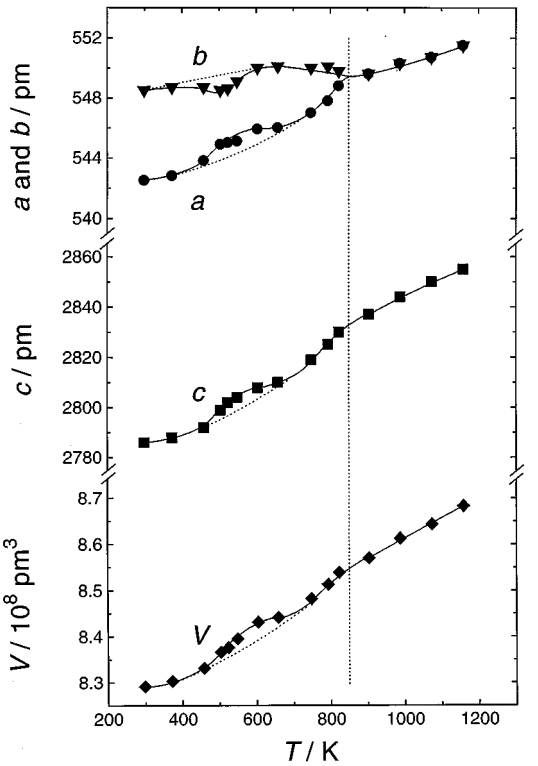

FIG. 3. Temperature dependence of the unit cell dimensions of $La_4Co_3O_{10.00}$ between 300 and 1200 K. Calculated standard deviations do not exceed size of symbols. Fully drawn lines are a guide for the eye.

(ii) Phase Transition, Thermal Expansion, and Oxidation

A structural phase transition from the monoclinic phase, possibly via an intermediate orthorhombic phase, to an apparently tetragonal phase is observed at 840 K (Fig. 3). The phase transition temperature is independent of the oxygen content. This confirms the transition temperature reported by Le Coustumer *et al.* (22). The monoclinic splitting is observed as a broadening of the reflections on the high-temperature PXD films, but the resolution is not sufficient for determining the degree of the monoclinic splitting nor the existence range for a possible orthorhombic intermediate phase. Figure 3 shows significant irregularities in the temperature dependence of the unit cell dimensions in the temperature range 400–600 K. These effects are most pronounced for the compounds with low oxygen contents, $\delta = 0.00$ and 0.07, and are observed for samples heated in sealed, as well as in open, capillaries. The irregularities are, therefore, not caused by the oxidation in air of, e.g. $La_4Co_3O_{10.00}$ to $La_4Co_3O_{10+\delta}$, a process which occurs in the same temperature range when the sample is submitted to air (cf. TGA data in Fig. 4). Furthermore, an oxidation would, according to the synchrotron data, imply a decreased unit cell volume (cf. Table 2). The anomaly in the thermal expansion is probably connected with an electronic transition (see section (iii)). The volume thermal expansion coefficient (α_V) for $La_4Co_3O_{10.00}$ was estimated from the HT-PXD data, using a linear approximation, as $\alpha_V = V^{-1}(\Delta V/\Delta T) = 5.5 \times 10^{-5}\ K^{-1}$. This high volume thermal expansion coefficient is comparable to α_V for $LaCoO_3$, but considerably higher than α_V for $LaCrO_3$ (13).

The above results show that the RP-type structure can incorporate large amounts of excessive oxygen, relative to the stoichiometric composition $La_4Co_3O_{10.00}$, without major structural changes. Isobaric (constant $p(O_2)$) TGA experiments reveal the temperature and $p(O_2)$ dependence of the nonstoichiometry, Fig. 4. The oxidation of $La_4Co_3O_{10.00}$ to $La_4Co_3O_{10+\delta}$ is fast in air at temperatures between 500 and 600 K. However, on cooling the oxidized sample in air to room temperature a further continuous increase of the oxygen content is observed below 600 K, and the oxidation even proceeds at room temperature (see above). The ease of the reaction indicates that the LaO-layer (probably) easily facilitates oxygen transport. $La_4Co_3O_{10+\delta}$ is stable in air for $T < 1250$ K. For $T > 1250$ K it decomposes by oxidation to $LaCoO_3$ and La_2O_3, as shown by the second weight increment in Fig. 4. Any composition of $La_4Co_3O_{10+\delta}$ with oxygen nonstoichiometry in the range $0.00 \leq \delta \leq 0.30$ can thus be prepared by careful

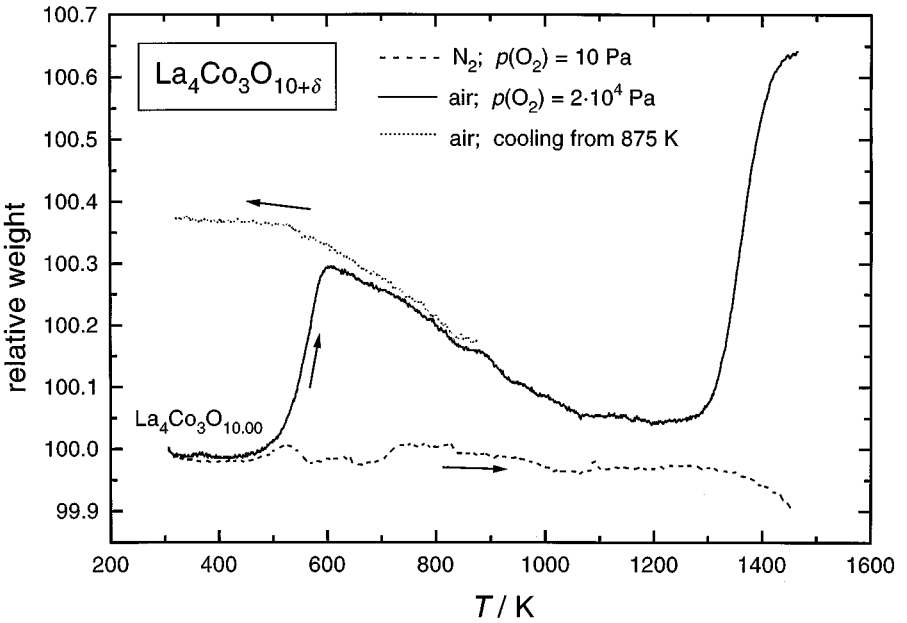

FIG. 4. TGA data showing weight change of $La_4Co_3O_{10+\delta}$ during heating (———) and cooling (.....) under $p(O_2) = 2 \times 10^4$ Pa (air), and during heating under $p(O_2) = 10$ Pa (N_2) (------). Starting composition $La_4Co_3O_{10.00}$. Heating rate 5 K min^{-1}.

control of temperature and $p(O_2)$. The oxygen content of $La_4Co_3O_{10.00}$ is essentially unchanged when heated in nitrogen up to approximately 1250 K. Above 1250 K the weight decreases, probably due to the loss of oxygen and, hence, indicating a small oxygen deficient non-stoichiometry, $La_4Co_3O_{10-\delta}$.

(iii) Magnetic Properties

Magnetic susceptibility (χ_m) data for $La_4Co_3O_{10+\delta}$ in the temperature region 2–985 K are presented in Figs. 5 and 6 and Table 4. Figure 5 shows the temperature dependence of the inverse molar susceptibility (χ_m^{-1}) for $\delta = 0.00$, 0.07, and 0.30. No difference was observed between cooling and heating experiments.

All $La_4Co_3O_{10+\delta}$ samples showed indications of antiferromagnetic ordering below $T_N \approx 13$ K (inset Fig. 5; T_N taken as the inflection point). The susceptibility maximum is most pronounced for $\delta = 0.00$ and 0.07. Further indications for long-range magnetic ordering was provided by powder neutron diffraction data which showed a few, very weak additional reflections at 1.7 K (31). Noteworthy, long-range antiferromagnetic ordering exists up to $T_N = 275$ K for La_2CoO_4 (10), the Co^{II}-representative in the RP-series ($n = 1$), whereas $LaCoO_3$ ($n = \infty$, Co^{III} d^6 low-spin ground state) shows no long-range magnetic ordering (29).

At temperatures above 20 K there are three regimes with nearly Curie–Weiss paramagnetic behaviour: 20–80 K, 100–450 K, 650–985 K (Fig. 5). Figure 6 shows the effect of magnetic field (H) on the inverse molar susceptibility for $2 \leq T \leq 100$ K. The samples with $\delta = 0.07$ and 0.30 show considerable deviations from Curie–Weiss behaviour at low fields, whereas at the higher fields a linear behaviour is approached. Stoichiometric $La_4Co_3O_{10.00}$ shows Curie–Weiss-like behaviour at all measured fields in this temperature interval. None of the samples shows any field dependence at temperatures above 100 K. Around 450 K a distinct change in $\chi_m^{-1}(T)$ occurs (see Fig. 5). For purposes of comparison, paramagnetic parameters calculated according to Curie–Weiss law for data measured at 5 kOe are given in Table 4. Values for $LaCoO_3$ are also included. A systematic variation in μ_P and Θ (Weiss constant) with oxygen content is found.

The deduced paramagnetic moments (μ_P) for $La_4Co_3O_{10+\delta}$ for the three temperature intervals indicate a temperature-induced change from a lower to a higher spin configuration. DSC (Fig. 7) and susceptibility measurements (Figs. 5, 6), performed on heating and cooling confirmed thermal reversibility of the changes. The susceptibility behaviour of $La_4Co_3O_{10+\delta}$ above 150 K is very similar to that reported for $LaCoO_3$ for which a magnetic/electronic transition around 500 K has been extensively discussed (11–14,18–20). Some characteristics related to the magnetic/electronic transitions in $La_4Co_3O_{10.00}$ and $LaCoO_3$ are compared in Fig. 7.

A proper discussion of temperature and composition induced variations in the paramagnetic moments is difficult,

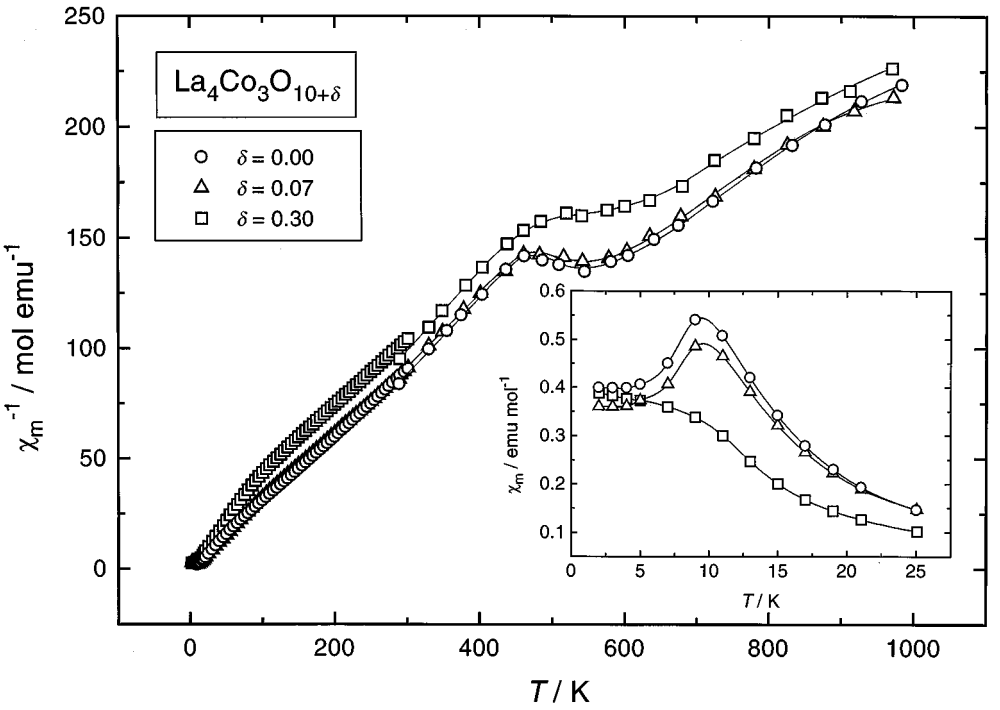

FIG. 5. Temperature dependence of the inverse molar magnetic susceptibility (χ_m^{-1}) for $La_4Co_3O_{10+\delta}$, measuring field $H = 5$ kOe. Inset shows susceptibility (χ_m) at low temperatures. Fully drawn lines are a guide for the eye.

since spin–orbital coupling is probably operative and different spin states can be close in energy. In $La_4Co^{II}Co^{III}_2O_{10}$, Co^{II} is probably high spin (HS, $S = 3/2$, spin only assumed), whereas octahedral Co^{III} is most probably low spin (LS, $S = 0$) at the lowest temperatures. Thus, the low temperature susceptibility for $La_4Co_3O_{10+\delta}$ is dominated by Co^{II}(HS), as indicated by the decreasing paramagnetic moment for increasing Co^{III}(LS) content at low temperature. Within the frame of the spin-only approximation, the expected paramagnetic moments (per formula units) are $3.87\mu_B$ for Co^{II}(HS)Co^{III}_2(LS), $5.57\mu_B$ for Co^{II}(HS)Co^{III}_2(IS) and $7.94\mu_B$ for Co^{II}(HS)Co^{III}_2(HS). The measured μ_P values, Table 4, are within this range of calculated values for all studied compositions. There exists convincing data for thermally induced spin transitions in $LaCoO_3$; LS → intermediate spin (IS) → HS (12,14–18), the ground state is assumed to be Co^{III}(LS) at 0 K. For $LaCoO_3$ and $La_4Co_3O_{10+\delta}$, increasing temperature probably favours a continuous transition towards IS/HS-states for Co^{III}, which is consistent with the observed increase in μ_P (Table 4). Co^{II} probably undergo no spin change in the actual temperature interval, consistent with findings for the related oxides La_2CoO_4 (10), $La_2Co_2O_5$ (32), and $La_4Co_3O_9$ (33), where long-range antiferromagnetic order of high spin Co^{II} ($S = 3/2$) prevails at low temperatures. The transition indicated by the magnetic susceptibility around 500 K for $La_4Co_3O_{10+\delta}$ (Fig. 5) is also manifested in the temperature dependence of the electric conductivity (23). For both $LaCoO_3$ and $La_4Co_3O_{10+\delta}$ the transition is interpreted as a semiconductor to metal transition (19, 20, 23). Contrary to $LaCoO_3$, the magnetic/electronic transition for $La_4Co_3O_{10.00}$ is clearly detected by DSC as an endothermal peak at 470 K (Fig. 7). Furthermore, for $La_4Co_3O_{10+\delta}$ the electronic transition is probably the cause for the coincident anomaly in the unit cell dimensions (Figs. 3 and 7). The spin conversion process for Co^{III}(LS) via IS to HS involves size changes for the Co species. Hence, the unusually large volume thermal expansion coefficient for $La_4Co_3O_{10.00}$ is an independent indication for a temperature-induced spin state change for Co^{III}.

The physical properties of $LaCoO_3$ have been extensively debated in the literature. Thus, the resemblance in behavior between $La_4Co_3O_{10+\delta}$ and $LaCoO_3$ as shown in Fig. 7 is particular interesting, considering the similarities and differences between their atomic arrangements. $LaCoO_3$ has the three-dimensional network of corner-sharing octahedra typical for the perovskite-type structure, whereas $La_4Co_3O_{10+\delta}$ has a two-dimensional network of perovskite-type triple layers (see Fig. 2). The interesting physical properties above 100 K for $La_4Co_3O_{10+\delta}$ and $LaCoO_3$ appear, hence, neither to depend strongly on three-dimensionality of the network of corner-sharing CoO_6 octahedra, the presence of substantial amounts of Co^{II}, nor on non-stoichiometry (for $La_4Co_3O_{10+\delta}$).

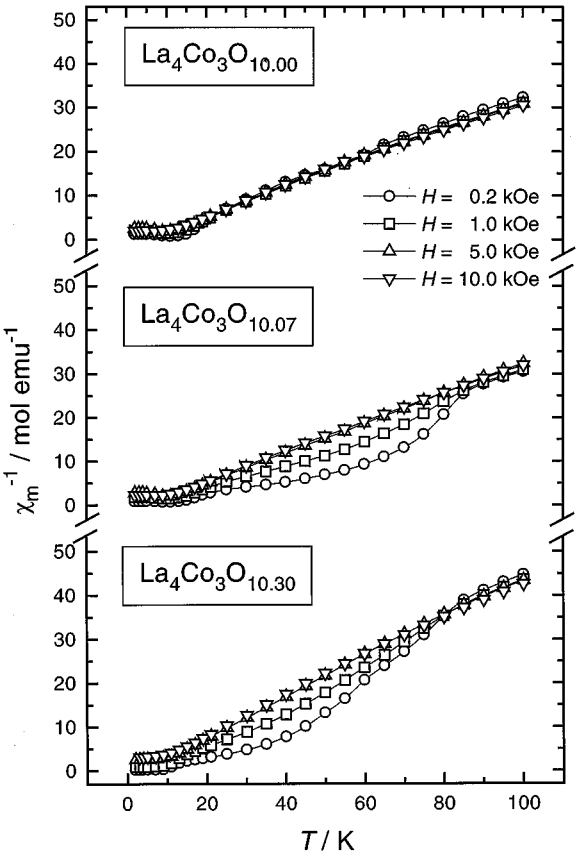

FIG. 6. Field and temperature dependence of the inverse molar magnetic susceptibility (χ_m^{-1}) for $La_4Co_3O_{10+\delta}$, $\delta = 0.00$, 0.07, and 0.30, $T < 100$ K. Fully drawn lines are a guide for the eye.

The field-dependent susceptibility for nonstoichiometric $La_4Co_3O_{10+\delta}$ ($\delta = 0.07$, 0.30) at $T < 100$ K (cf. Fig. 6) is much less pronounced than reported for $LaCoO_3$ (13). Saturation of the field-dependent susceptibility occurs for $H > 5$ kOe for $La_4Co_3O_{10+\delta}$. It has been proposed that the field-dependent susceptibility of $LaCoO_3$ stems from ferromagnetic clusters with origin in either Co^{II} or Co^{IV} specimens,

TABLE 4
Paramagnetic Properties of $La_4Co^{II}_{(1-2\delta)}Co^{III}_{(2+2\delta)}O_{10+\delta}$

	Composition			20–80 K		100–300 K		620–920 K	
δ	Co^{II} $(1-2\delta)$	Co^{III} $(2+2\delta)$	T_N (K)	μ_P (μ_B)	Θ (K)	μ_P (μ_B)	Θ (K)	μ_P (μ_B)	Θ (K)
0.00	1	2	13	4.9	4	5.2	− 2	6.2	− 72
0.07	0.86	2.14	13	4.8	5	5.3	− 12	6.5	− 159
0.30	0.40	2.60	13	4.1	4	5.2	− 47	6.7	− 291
$(LaCoO_3)_3$[a]	0	3				5.9	− 185	7.1	− 504

Note. Values for $20 \leq T \leq 80$ K refer to measurements in magnetic field $H = 5$ kOe. μ_P given per formula unit.

[a] Moments calculated from data in Ref. 11.

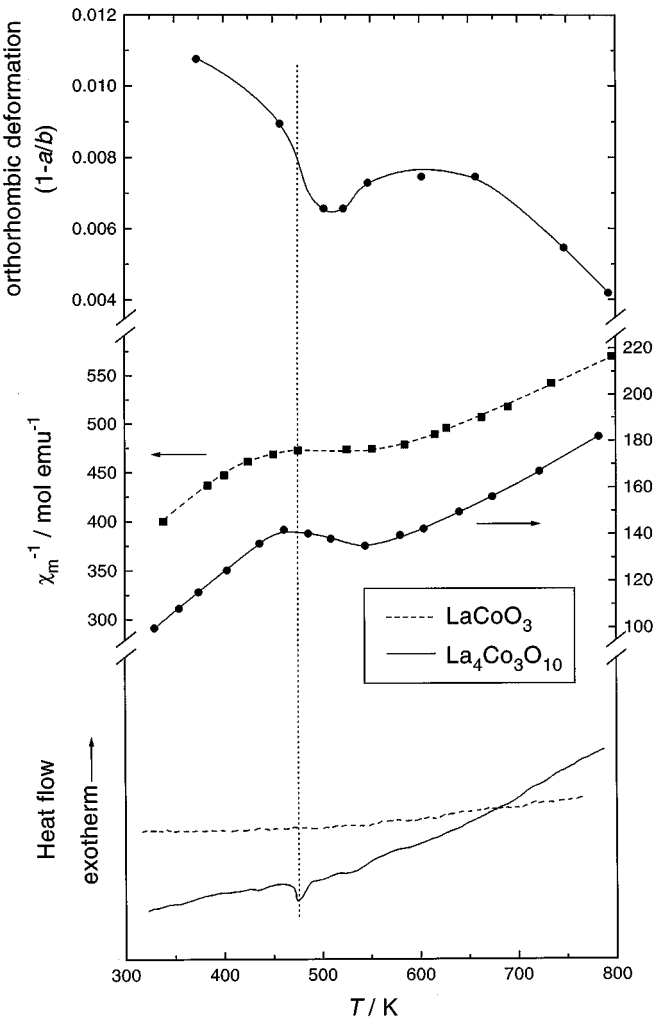

FIG. 7. Comparison of temperature-induced changes in unit cell dimensions, magnetic susceptibility, and DSC signal in connection with the electronic transition in $La_4Co_3O_{10.00}$ (solid lines) and $LaCoO_3$ (dashed lines, from Refs. (13) and (25). Fully drawn lines are a guide for the eye.

existing due to incomplete oxidation or as charge compensation owing to divalent impurities on the La site (13). Since the phenomenon is also observed in $La_4Co_3O_{10+\delta}$ with a lower average oxidation state for cobalt, other explanations must be sought. Furthermore, the magnetic Co^{II}—Co^{II} and Co^{II}—Co^{III} interactions in oxides are predominantly antiferromagnetic (cf. the antiferromagnetic order in La_2CoO_4 (10), $La_2Co_2O_5$ (32), $La_4Co_3O_9$ (33), and presently $La_4Co_3O_{10+\delta}$). The field-dependence of the susceptibility for $La_4Co_3O_{10+\delta}$ seems to correlate with the amount of Co^{III}. The field-dependent susceptibility of $LaCoO_3$ at $T < 100$ K has alternatively been explained as an intrinsic property of the compound, correlated with the mixed LS and IS states for Co^{III} (13). The possibility of ferromagnetic clusters of, e.g. Co^{III}(IS), would be consistent with the field-dependent susceptibility. For $La_4Co_3O_{10+\delta}$ the interactions

and/or clustering between different Co^{III} species is reduced with decreasing oxygen content, since Co^{III} is diluted with Co^{II}. In addition, for the layered RP-structure of $La_4Co_3O_{10+\delta}$ the number of indirect Co^{III}—O—Co^{III} exchange pathways, which possibly could be important for the interactions leading to the formation of ferromagnetic clusters of Co^{III}(IS) or Co^{III}(HS), is less than in the three-dimensional $LaCoO_3$ structure.

ACKNOWLEDGMENTS

This work has received financial support from the Research Council of Norway. Contribution 98.6 from the Swiss–Norwegian Beam Line at ESRF. The skillful assistance from the project team at the Swiss–Norwegian Beam Line, ESRF, is gratefully acknowledged.

REFERENCES

1. S. N. Ruddlesden and P. Popper, *Acta Cryst*. **11,** 54 (1958).
2. A. Demourgues, F. Weill, B. Darriet, A. Wattiaux, J. C. Grenier, P. Gravereau, and M. Puchard, *J. Solid State Chem.* **106,** 317 (1993).
3. Z. Zhang, M. Greenblatt, and J. B.Goodenough, *J. Solid State Chem.* **108,** 402 (1994).
4. K. Sreedhar, M. McElfresh, D. Perry, D. Kim, P. Metcalf, and J. M. Honig, *J. Solid State Chem.* **110,** 208 (1994).
5. Z. Zhang and M. Greenblatt, *J. Solid State Chem.* **117,** 236 (1995).
6. C. Park and R. L. Snyder, *J. Amer. Ceram. Soc.* **78,** 3171 (1995).
7. J. J. Janecek and G. P. Wirtz, *J. Amer. Ceram. Soc.* **61,** 242 (1978).
8. M. Seppänen, M. Kytö, and P. Taskinen, *Scand. J. Metall.* **8,** 199 (1979).
9. K. Kitayama, *J. Solid State Chem.* **73,** 381 (1988).
10. K. Yamada, M. Matsuda, Y. Endoh, B. Keimer, R. J. Birgeneau, S. Onodera, J. Mizusaki, T. Matsuura, and G. Shirane, *Phys. Rev. B* **39,** 2336 (1989).
11. M. A. Señarís-Rodríguez and J. B. Goodenough, *J. Solid State Chem.* **116,** 224 (1995).
12. S. Stølen, F. Grønvold, H. Brinks, T. Atake, and H. Mori, *Phys. Rev. B* **55,** 14103 (1997).
13. B. G. Tilset, H. Fjellvåg, A. Kjekshus, and B. C. Hauback, *Acta. Chem. Scand.* **52,** 733 (1998).
14. T. Saitoh, T. Mizokawa, A. Fujimori, M. Abbate, Y. Takeda, and M. Takano, *Phys. Rev. B* **55,** 4257 (1997).
15. S. Yamaguchi, Y. Okimoto, and Y. Tokura, *Phys. Rev. B* **55,** R8666 (1997).
16. M. Itoh, M. Mori, M. Sugahara, T. Yamauchi, and Y. Ueda, *Physica B* **230–232,** 756 (1997).
17. K. Asai, O. Yokokura, M. Suzuki, T. Naka, T. Matsumoto, H. Takahashi, N. Mori, and K. Kohn, *J. Phys. Soc. Jpn.* **66,** 967 (1997).
18. M. A. Korotin, S. Yu. Ezhov, I. V. Solovyev, and V. I. Anisimov, *Phys. Rev. B* **54,** 5309 (1996).
19. G. Thornton, B. C. Toefield, and D. E. Williams, *Solid State Commun.* **44,** 1213 (1982).
20. S. Yamaguchi, Y. Okimoto, H. Taniguchi, and Y. Tokura, *Phys. Rev. B* **53,** R2928 (1996).
21. M. Seppänen and M.H. Tikkanen, *Acta Chem. Scand. A* **30,** 389 (1976).
22. L. R. Le Coustumer, Y. Barbaux, J. P. Bonnelle, P. Conflant, J. Loriers, and F. Clerc, *C.R. Acad. Sci. Paris Ser. II* **292,** 953 (1981).
23. L. R. Le Coustumer, Y. Barbaux, and J. P. Bonnelle, *Nuov. J. Chim* **6,** 7 (1982).
24. F. Grigsdies and R. Schöllhorn, *Solid State Commun.* **91,** 111 (1994).
25. B. Gilbu, H. Fjellvåg, and A. Kjekshus, *Acta Chem. Scand.* **48,** 37 (1994).
26. B. Noläng, "Program UNITCELL," Department of Chemistry, Uppsala University, Sweden.
27. A. C. Larson and R. B. Von Dreele, *GSAS General Structure Analysis System*, LANSCE, MS-H 805, Los Alamos National Laboratory, Los Alamos, NM 87545, USA.
28. J. Spreadborough and J. W. Christian, *J. Sci. Instrum.* **36,** 116 (1959).
29. G. Thornton, B. C. Toefield, and A. H. Hewat, *J. Solid State Chem.* **61,** 301 (1986).
30. U. Lehman and Hk. Müller-Buschbaum, *Z. Anorg. Allg. Chem.* **470,** 59 (1980).
31. O. H. Hansteen, H. Fjellvåg, and B. C. Hauback, *Chem., Papers*, in press.
32. O. H. Hansteen, H. Fjellvåg, and B. C. Hauback, *J. Solid State Chem.*, press.
33. O. H. Hansteen, H. Fjellvåg, and B. C. Hauback, *J. Mater. Chem.*, press.